Applied Energy 210 (2018) 1251–1265

Contents lists available at ScienceDirect

Applied Energy

journal homepage: www.elsevier.com/locate/apenergy

Enabling resilient distributed power sharing in networked microgrids through software defined networking

Lingyu Ren [a], Yanyuan Qin [b], Yan Li [a], Peng Zhang [a,*], Bing Wang [b], Peter B. Luh [a], Song Han [b], Taofeek Orekan [a], Tao Gong [b]

[a] Dept. of Electrical and Computer Engineering, University of Connecticut, Storrs, CT 06269, USA
[b] Dept. of Computer Science and Engineering, University of Connecticut, Storrs, CT 06269, USA

HIGHLIGHTS

- An SDN-enabled control and communication architecture is established for NMGs.
- A resilient distributed power sharing control strategy is devised for NMGs.
- Novel event-triggered communication is deployed through an SDN architecture.
- A cyber-physical HIL testbed is built to validate NMGs' control and communication strategies.

ARTICLE INFO

Article history:
Received 31 March 2017
Received in revised form 22 May 2017
Accepted 7 June 2017
Available online 16 June 2017

Keywords:
Networked microgrids
Software-defined networking
Event-triggered communication
Distributed power sharing

ABSTRACT

Networked Microgrids (NMGs) offer a new, more resilient alternative to traditional individual Microgrids (MGs). Even though networking existing microgrids presents clear advantages, the scalable and resilient communication and control infrastructure necessary for supporting this innovation does not yet exist. This paper addresses this challenge by developing a Software-Defined Networking (SDN) enabled architecture that can achieve fast power support among microgrids, transforming isolated local microgrids into integrated NMGs capable of achieving the desired resiliency, elasticity and efficiency. Equipped with a novel event-triggered communication scheme, the SDN-based architecture enables distributed power sharing among microgrids in both the transient period and the steady state, a capability that is unattainable using existing technologies. Extensive experiments on a cyber-physical Hardware-in-the-Loop (HIL) NMGs testbed have validated the effectiveness and efficiency of the SDN-enabled distributed power sharing method.

1. Introduction

A microgrid normally refers to a localized autonomous distribution network designed to supply electrical and heat loads for a local community (e.g., a university campus [1], a commercial building [2] or a residential area [3]). It can be connected with the main grid (*grid connected mode*) or isolated during main grid emergencies (*islanded mode*). Because microgrids offer the following benefits, they have attracted increased interest in the last few years: they enable integration and coordination of renewable energy resources; they enhance the resilience of electrical system for customers; and they reduce economic and emission costs [4]. These benefits are particularly important given the rapid development of power electronics technologies as well as primary, secondary and tertiary control techniques in recent years [5].

The swift growth of microgrid research and development are leading to increased penetration of microgrids [6]. For instance, in urban areas where populations and critical loads are concentrated, microgrids are being increasingly deployed. A smart city (or smart and connected communities) zone is expected to have many microgrids operated by various stakeholders. It is therefore natural to ask whether coordinated networked microgrids can offer a more resilient system than individual microgrids. Indeed, our preliminary research [7] shows that, when local microgrids are networked, this not only enables faster distribution grid recovery during a main grid blackout but also significantly improves the system's day-to-day reliability. In fact, the U.S. Department of Energy

* Corresponding author.
E-mail address: peng.zhang@uconn.edu (P. Zhang).

http://dx.doi.org/10.1016/j.apenergy.2017.06.006
0306-2619/

Nomenclature

Acronyms

NMGs	networked microgrids
MG	microgrid
SDN	software-defined networking
HIL	hardware-in-the-loop
DG	distributed generator
ACA	average consensus algorithm
LC	local controller
PCC	point of common coupling
DAPI	distributed-averaging proportional-integral
VM	virtual machine
VSC	voltage source converter
PWM	pulse-width modulation
K-NN	K-nearest neighbors

Indices

i	index for MGs
j	index for DGs
l	index for neighboring DGs
k	index for neighboring MGs

Sets

$\mathscr{V}$	set of MGs
$\mathscr{V}_i$	set of DGs in the ith MG
$\mathscr{L}_j$	Set of neighboring DGs of the jth DG
$\mathscr{K}_i$	Set of neighboring MGs of the ith MG

anticipates that researching and developing of networked microgrids will usher in the next wave of smart grid technology. This innovative approach promises to meaningfully modernize the nation's grid system in response to issues such as climate change and the need for greater grid resilience [8].

Though networking existing microgrids offers a number of advantages, there is one major challenge that has not been addressed: a scalable and resilient communication and control infrastructure does not yet exist. Furthermore, given the standardized control architecture of individual microgrids (e.g., droop control, secondary control), it is highly desirable to establish a network-level control architecture that does not significantly modify the communication and control layers in individual microgrids. This paper aims to address these challenges by developing an SDN-enabled architecture that can readily network microgrids at the cyber layer in a simple and economically efficient way, transforming isolated local microgrids into integrated smart microgrids capable of achieving the desired resiliency, elasticity and efficiency. In particular, this novel method will enable a provably correct and previously unattainable distributed power sharing among microgrids in both the transient period and the steady state.

Related work: Networked microgrids, or coupling microgrids, can be defined as a cluster of microgrids interconnected in close electrical or spatial proximity with coordinated energy management and interactive support and exchange. Recently, the feasibility of coupling microgrids through common AC buses [9], utility feeders [10] and DC links [11] has been discussed. Ref. [12] presents a power dispatch strategy for maintaining islanded microgrids' power balances through microgrid generation reallocation triggered by power deficiency events. Ref. [13] presents the use of networked microgrids to improve the self-healing of the distribution network under power outages, where microgrids are designed to pick up external loads with minimum switch operations. Further, an economic dispatch strategy for networked microgrids is developed [14], where the surplus capacities in individual microgrids are aggregated to fulfill the power requirements. Apart from facilitating power system restoration, networked microgrids can also participate in global frequency regulation by providing extra frequency control reserves [15]. The interaction between the distribution network operator and local microgrids has also been investigated [16,17]. These studies focus on the longer-term coordination of interconnected microgrids at a time scale of minutes, hours or longer. In the real world, however, microgrids usually have low inertia and intermittent renewable generation. Thus, it is critically important to ensure fast power sharing while maintaining transient stability in networked microgrids. In order to adequately control such a complex system, a high-speed, resilient cyber infrastructure is indispensable, but this remains an open challenge.

In networked microgrids, one of the most important functions is to share power demands among the networked Distributed Generators (DGs). Power sharing in a single microgrid is achieved in tandem with voltage and frequency recovery either in a centralized or a distributed way [18,19]. The latter has been attracting more attentions in recent years due to the potential benefits of avoiding the single point of failure and reducing communication overhead [20,21]. In [22], a distributed control requiring only local communication is presented, which is capable of achieving proportional active power sharing and frequency restoration. This paper also identifies the conflict between voltage control and reactive power sharing for DG units with a droop-based primary control. An alternative approach for fast voltage recovery without considering reactive power sharing is developed in [23]. Among various distributed power sharing schemes, the Average Consensus Algorithm (ACA) is a popular choice for solving the problem in a fully distributed fashion. ACA, however, can compromise network resilience by requiring continuous intensive data transmissions which may cause bandwidth shortage, congestion, and processor overuse. Moreover, there is a lack of distributed power sharing schemes for networked microgrids in the existing literature.

Our contributions: To enable resilient networked microgrids and close the aforementioned gaps, we are introducing a novel SDN-based cyber architecture with a distributed event-triggered communication scheme. The authors have pioneered the use of SDN in enabling resilient microgrids [24] by devising a novel SDN-based cyber architecture for individual microgrids and developing SDN functions such as delay management, automatic failover, and traffic prioritization. The unprecedented flexibility and dynamic programmability of SDN [25–27] supports on-the-fly network updates and enables the interoperability of local microgrids. Therefore, the SDN-based architecture in [24] is further expanded to enable networked microgrids. We also integrate the event-triggered communication in the SDN-based communication architecture such that a microgrid only shares information with its neighbors when the specific states exceed predefined thresholds. Recent research into networked control systems has mathematically proven the effectiveness of the event-triggered communication in enabling more efficient and robust ACAs [28–30]. This paper makes three main contributions:

- It devises a layered cyber and control architecture that supports the plug-and-play of networked microgrids. The local layer includes the primary and secondary controllers within individual microgrids while the global layer is responsible for the

dynamic power sharing among different microgrids. This new architecture requires little modification in individual microgrids and enables seconds-level fast power support among microgrids.

- It develops the SDN-enabled event-triggered communication scheme in the global layer. Power deficiency and its recovery are defined as "events" which are detected locally in the DGs and sent to the SDN controller. Once it receives these requests, the SDN controller will use an electrical distance matrix to find the closely coupled microgrids cluster and update the corresponding communication network. In this way, global data transmission is only required during triggered periods, which significantly reduces communication costs and enhances the system's resiliency.
- It builds a cyber-physical HIL testbed that validates the effectiveness and efficiency of the new architecture and the distributed power sharing method for networked microgrids. The new testbed will serve as a powerful instrument for developing advanced analytics and controllers for future networked microgrid research.

The remainder of the paper is organized as follows: Section 2 presents the distributed power sharing control for networked microgrids. Section 3 elaborates the SDN-enabled event-triggered communication methods. Section 4 introduces a cyber-physical HIL NMGs testbed, and Section 5 summarizes the experimental results that validate the effectiveness of the distributed power-sharing scheme for NMGs. Finally, Section 6 concludes the whole paper.

2. Distributed power sharing for networked microgrids

It is assumed that, in islanded NMGs, each MG is equipped with only local controllers (LCs) on inverter-interfaced DGs. Droop controllers are used as the primary control for automatically adjusting its power output under demand changes. To achieve local power sharing, the distributed-averaging proportional-integral (DAPI) control [22] is applied to these LCs as a secondary control due to its flexibility and scalability. In this section, a droop control and a local power-sharing algorithm are first reviewed, and then an average-consensus-based global power sharing control is presented to provide fast power support among microgrids. The effectiveness and limitations of this two-layered power-sharing scheme is discussed, motivating the subsequent event-triggered communication design in Section 3.

2.1. Preliminaries

Consider a group of NMGs consisting of N microgrids labeled as $\mathscr{V} = \{1, \ldots, N\}$. For the i^{th} microgrid, there are N_i controllable DGs (microturbines, diesel generators or combined heat and power units, etc.), indexed as $\mathscr{V}_i = \{1, \ldots, N_i\}$. The communication network for the ith microgrid can be represented as an undirected graph $G_i = \{\mathscr{V}_i, \mathscr{E}_i, A_i\}$, where $\mathscr{E}_i \subseteq \mathscr{V}_i \times \mathscr{V}_i$ is the edge set (refers to the cyber connections between DGs in microgrid i) and A_i is the adjacent matrix with the binary element set $\{a^i_{mn}\}$. a^i_{mn} is 1 if the edge $\{m, n | m, n \in \mathscr{V}_i\}$ exists; otherwise, it is 0. Similarly, the communication among microgrids can be expressed as $G = \{\mathscr{V}, \mathscr{E}, A\}$, where $\mathscr{E} \subseteq \mathscr{V} \times \mathscr{V}$ refers to the cyber connections between microgrids and A is the corresponding adjacent matrix.

The communication among microgrids is established through the LCs' transceivers. It is assumed that the individual microgrids already have a local connected communication network but that a dedicated interface for communication with other microgrids is needed. For this reason, one of the DGs is selected as the leader DG for each microgrid i. It is through the leader DG's transceiver that the microgrids share information with one another. The leader DG is designed for its fast response to the power support request; thus, in practice, the DG with the largest capacity is selected as the leader DG. Without a loss of generality, the leader DG can be numbered as the first DG in the node set $\mathscr{V}_i$. The ith DG set can accordingly be specified as $\mathscr{V}_i = \{1, \mathbf{2}, \ldots, \boldsymbol{N_i}\}$ with the bold index referring to the follower DGs. An example of islanded NMGs with 3 MGs and multiple distributed DGs is shown in Fig. 1.

2.2. A review of droop control and DAPI control

Droop control. The general expression of a droop m_j controller on the jth DG in the ith microgrid is described as:

$$f_j = f^* - m_j\left(P_j - P_j^*\right) = f_j^* - m_j \Delta P_j, \quad j \in \mathscr{V}_i \tag{1a}$$

$$E_j = E_j^* - n_j\left(Q_j - Q_j^*\right) = E_j^* - n_j \Delta Q_j, \quad j \in \mathscr{V}_i \tag{1b}$$

where f_j and E_j are the frequency and voltage magnitude of the jth DG, f^* and E_j^* being their references. P_j and Q_j are the active power and reactive power, P_j^* and Q_j^* being their references and ΔP_j and ΔQ_j as the corresponding power error inputs for the droop controller. m_j and n_j are the frequency droop coefficient and the voltage droop coefficient respectively. To get proportional power sharing, the frequency droop coefficients are defined to be inversely proportional to their corresponding power ratings, i.e., $m_{j1}/m_{j2} = P_{j2}^*/P_{j1}^*$.

According to an analogical analysis between the frequency droop coefficient and the inverse of the damping factor in an oscillator, the system frequency's synchronization is provably guaranteed when the power injections and power flows are below their physical maximums [31,32]. For the voltage droop control, one essential challenge is that the feeder impedance between the inverter and the PCC bus greatly affects its steady state operation point. Even though advanced accurate reactive power controls such as the error compensation control [33] and the adaptive impedance control [34] are presented, both methods need a central controller and are thus unsuitable for distributed power sharing. This paper focuses on the precise sharing of the real power rather than the reactive power; thus, the trade-off between voltage regulation and reactive power sharing is performed using DAPI.

One drawback of droop control is that changes in load power will cause voltage and frequency to deviate from their set points. Fig. 2 depicts the Q-E and P-f droop characteristics with steady state points A, B, A′, and B′. The graph shows that droop characteristics lead to poor frequency and voltage performance in the steady state. For frequency droop, A′ and B′ can be calculated through (1a) and the steady state synchronization frequency $f_{ss} = f^* - \frac{\sum P_j}{\sum 1/m_j}$. However, as discussed earlier, for the voltage droop, the calculation of operation points A and B is determined jointly by the load level, the feeder impedance, and the droop coefficient. To eliminate this deviation, a secondary control is needed.

Here, we introduce the DAPI controller, an average consensus based integral controller that allows for secondary control, which eliminates the frequency and voltage deviations caused by the primary droop control. The mathematical formulation of DAPI for the jth DG in the ith microgrid is:

$$f_j = f^* - m_j\left(P_j - P_j^*\right) + F_j, \quad j \in \mathscr{V}_i \tag{2a}$$

$$F_j = -\int \{\alpha_j\left(f_j - f_j^*\right) + \sum_{l \in \mathscr{L}_j} \beta_{lj}(F_j - F_l)\}, \quad j \in \mathscr{V}_i \tag{2b}$$

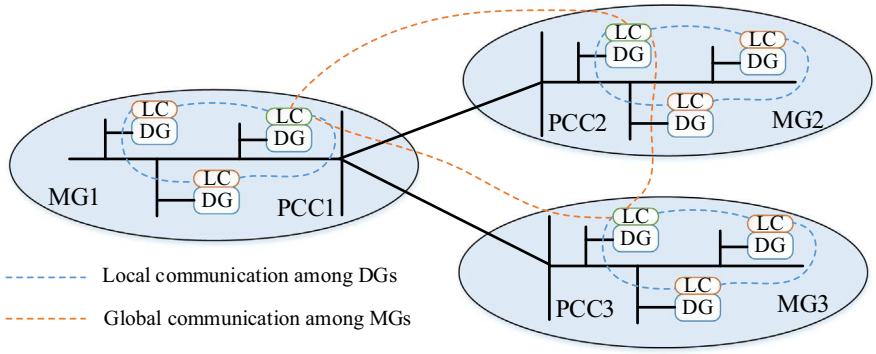

Fig. 1. An example of networked microgrids. (Green LCs: LCs of the leader DGs; Orange LCs: LCs of the follower DGs; PCC: point of common coupling).

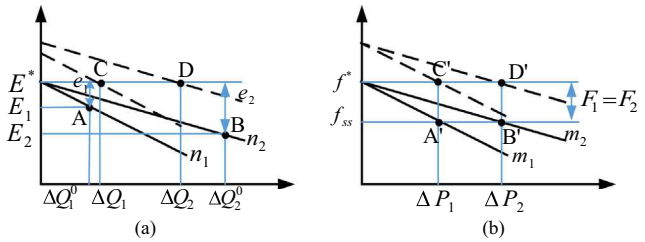

Fig. 2. Performance of the DAPI illustrated by droop curve.

$$E_j = E_j^* - n_j\left(Q_j - Q_j^*\right) + e_j, \quad j \in \mathcal{V}_i \tag{3a}$$

$$e_j = -\int\{\gamma_j\left(E_j - E_j^*\right) + \sum_{l\in\mathcal{L}_j}\delta_{lj}(Q_j/Q_j^* - Q_l/Q_l^*)\}, \quad j \in \mathcal{V}_i \tag{3b}$$

where F_j and e_j are respectively the secondary frequency control variable and the secondary voltage control variable and $\mathcal{L}_j \subseteq \mathcal{V}_i$ is the neighboring DG set of the jth DG. This set is determined by the local communication network in microgrid i, which corresponds to the nonzero elements on the jth row or column in the adjacent matrix A_i. The control parameters related to frequency and voltage restoration are denoted by α_j and γ_j while β_{lj} and γ_{lj} are related to active and reactive power sharing. To obtain desirable results, the parameters shall be tuned as detailed in [22]. The steady state performance of the DAPI controller is illustrated in Fig. 2. The droop controlled operation points A, B, A′, and B′ are shifted to C, D, C′, and D′ respectively. It can be proven that the stabilized secondary frequency control variable F of all DGs will be unified while the secondary voltage control variable e will not accurately be equal to each other due to the impedance mismatch (Fig. 2(a) shows only one possible result).

2.3. Global layer active power sharing for networked microgrids

2.3.1. Global layer active power sharing

In this section, global layer active power sharing is discussed. By implementing a DAPI controller, each microgrid in an NMGs community has the capability of local power sharing in a distributed manner without the central controller or the one-to-all communication being required. Still, microgrids should be able to share information to participate in community-level power exchanges to fulfill the benefits expected from microgrids' interconnection. However, in order to avoid violating the best local performance of the microgrids after they are physically networked, their local controller parameters must remain unchanged.

In this paper, we present an innovative way to achieve fast global power sharing. First, the following basic assumptions are made:

(1) The microgrids are connected through AC feeders;
(2) DGs in a single microgrid are coupled more strongly than DGs in different microgrids;
(3) The reactive power is not shared among microgrids.

The first assumption is justifiable, as it is economically affordable to use existing distribution system facilities, such as medium- or low-voltage feeders, rather than inverter-based DC links for connecting multiple microgrids. Also, most prior research utilizes medium-voltage distribution feeders as a backbone for networking microgrids. This method might not be preferable under islanded mode when the consumers on the backbone are not critical loads but have to be fed due to the microgrids integration. In our scenario, we assume the microgrids are connected through distribution power lines with no loads in the middle, which means that the NMGs are geographically close.

Hence, the second assumption is validated since the DGs are linked through extra feeders with those in other microgrids. As an aforementioned conclusion, the local droop controller can achieve proportional power sharing via frequency synchronization. The time constant of this synchronization depends partly on the strength of the electrical connection between any two DGs. Intuitively, the closely coupled DGs will converge faster than those that are loosely connected.

Furthermore, based on the small signal analysis of the DAPI method's reactive power sharing [22], the dissimilarity among DGs (including interconnected line impedance) will cause instability. Also, it is physically not favored to do long-distance reactive power sharing, which will likely cause a severe voltage problem. Instead, local reactive power compensation can be adopted by using a shunt capacitor or STATCOM. Thus, we do not take global reactive power sharing into consideration.

Global active power sharing is implemented on the leader DG. For the ith microgrid, it is formulated as:

$$F_1 = -\int\left\{\alpha_1(f_1 - f^*) + \sum_{l\in\mathcal{L}_1}\beta_{l1}(F_1 - F_l)\right\} - \int\left\{\sum_{k\in\mathcal{K}_i}\eta_{ki}(F_1 - F_k)\right\}, \quad 1 \in \mathcal{V}_i \tag{4}$$

where $\mathcal{K}_i \subseteq \mathcal{V}$ is the neighboring microgrids set of microgrid i; η_{ki} is the control parameter related to global active power sharing. Compared with Eq. (2b), except for the existing frequency restoration control and local power sharing control, an additional global power

sharing control is added to balance power between neighboring microgrids. No changes are required for the follower DGs. The overall structure is shown in Fig. 3.

2.3.2. Effectiveness and limitations

Two-layered power sharing is an approach for unifying the steady state value of the secondary frequency variable F for DGs not only in a single MG but also in its neighboring MGs. As shown in Fig. 2(b), in a steady state, the system must achieve $f_j = f^*$ and $F_j = F_l,\ l \in \mathscr{L}_j$. With a global control, it is forced to also achieve $F_j = F_k,\ k \in \mathscr{K}_i$. Thus, we have $F_j = F_k = F_l,\ l \in \mathscr{L}_j,\ k \in \mathscr{K}_i$. Since the local layer DAPI method requires a connected communication graph $(G_i,\ i \in \mathscr{V})$, the above relation is applied on DGs in MG and all its neighboring MGs. Finally, we can achieve power sharing among neighboring microgrids.

Two-layered power sharing for NMGs is an extension of the DAPI control for single microgrids. Based on the analysis in [21], the power sharing control, involving partial or all inverters, does not cause instability for the droop control based system. This conclusion applies to NMGs. However, the AC lines between microgrids generate greater impedance, which will slow down synchronization and further decelerate the convergence of the power sharing process. Therefore, it is necessary to identify a proper set of neighboring MGs for each MG, which will provide fast power support. Instead of involving all MGs in the global power sharing layer, neighboring microgrid set is more efficient and favorable for achieving the scalability and plug-and-play for the NMGs.

The level of communication entailed in the global power sharing control requires an investment in extra bandwidth and maintenance and will possibly cause system disorder due to congestion, large delays, or link failures. To minimize the risk and cost of global communication, a flexible communication infrastructure that supports dynamic network configuration based on power sharing requests is highly necessary.

3. SDN-enabled event-triggered communication

This section outlines how SDN-enabled and event-triggered communication is designed for global layer power sharing among selected microgrids with close electrical distances. Studies have shown that large communication latency in microgrid operation with a centralized secondary control can cause undesired control deviations and even stability concerns [35,36]. Also, the performance of the ACA with communication delays is discussed in [37], showing that the ACA only converges when the latencies are below certain levels. Communication strategies with less delay and congestion are therefore crucial in microgrid control. In the following, we first briefly introduce the electrical distance for determining microgrid clusters, then we provide a detailed description of an event-triggered communication solution using an SDN architecture.

3.1. Electrical distance based microgrid power sharing cluster

As shown in Fig. 3, the NMGs are configured in such a way that each microgrid is connected with the electrical power network through a point of common coupling (PCC) bus. The strength of the microgrid coupling is examined via the concept of electrical distance, which has already been used for subsystem partitioning in bulk power systems. For the P-f droop control, active power is regulated by frequency variation via the consequent voltage angle difference. Furthermore, as indicated by the DC power flow model, the susceptance matrix represents the sensitivity of active power changing with respect to voltage angle variance. Therefore, we adopt the idea of "reactance distance" as the electrical distance among MGs to reflect the strength of the droop control effect.

Let $\boldsymbol{B}$ be the susceptance matrix of the electrical power network that connects different MGs and $\boldsymbol{B}^+$ be its pseudo inverse. Then the reactance distance d_{ki} between PCC bus k and PCC bus i can be expressed as Eq. (5) [38]:

$$d_{ik} = (\boldsymbol{B}^+)_{kk} - (\boldsymbol{B}^+)_{ki} - (\boldsymbol{B}^+)_{ik} + (\boldsymbol{B}^+)_{ii} \tag{5}$$

Let $D = \{d_{ki}\}$ be the electrical distance matrix. By selecting K smallest elements in the ith row (excluding the diagonal elements), a K-nearest neighbors (K-NN) microgrid cluster can be determined. Accordingly, the global fast active power sharing is implemented in the K-NN microgrid cluster centered on the microgrid with power shortage.

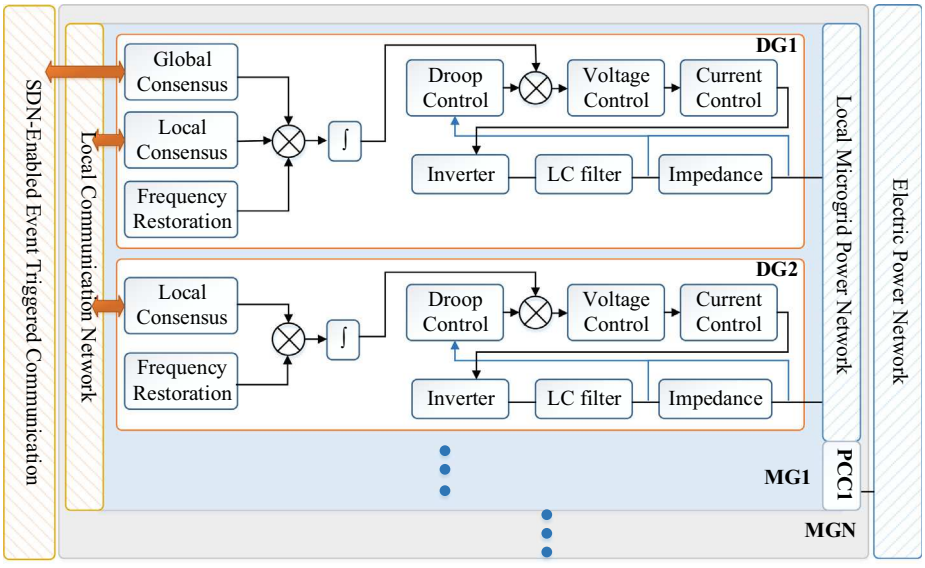

Fig. 3. Scheme of the two-layered power sharing control for networked microgrids.

3.2. SDN-enabled event-triggered communication for global power sharing

Power sharing among microgrids is only required when the demand change exceeds a threshold such that there is an emergency state in the individual microgrids. The threshold can be determined based on the specific conditions of the networked microgrids (e.g., the reserved capacity of each individual microgrid) and on customer needs. Here, we show an example of 20% of the nominal microgrid power output.

3.2.1. Event detection

Let $E1$ and $E2$ represent two types of "events" where $E1$ is defined as a global power sharing request from local microgrids and $E2$ is the request clearance after power sharing is achieved. These events are detected on the local controllers.

An $E1$ event is triggered under two scenarios: a large demand increase and its recovery. To detect an event, the active power error signal $\Delta P_j = P_j - P_j^*,\ j \in \mathscr{V}_i$ from the droop controller of the jth DG is compared with a predefined threshold $P_{th}^i = 20\% P_{total}^i$ where P_{total}^i is the sum of all the nominal power ratings of microgrid and is assumed to be known by all DGs in the parameter initialization process. If $\Delta P_j > P_{th}^i$, it indicates that there is a sudden demand surge and its value is beyond the predefined threshold, which leads to an overloading issue in an individual microgrid. In this case, the local controller will send an $E1$ request to prompt global power sharing control. Likewise, if $\Delta P_j < -P_{th}^i$ after the surge, it shows the demand has been recovered and an $E1$ request is also required to bring down the power contribution from neighboring microgrids through global power sharing.

As for an $E2$ event, it is triggered when power sharing is achieved at an acceptable level after a large demand increase or its recovery. Since the power sharing process is accompanied by frequency restoration, to detect $E2$, the frequency error signal $\Delta f_j = f_j - f_j^*,\ j \in \mathscr{V}_i$ is utilized. When the absolute value of Δf_j is restored to $\Delta f_j^{th} = m_j * P_{th}^i/(\mathrm{K}+1)$, the demand is reduced to a desired level. Then global communication can be canceled through the SDN network.

To keep the above process in order, a detection sequence is needed. In particular, demand recovery $E1$ events should only be detected after the demand surge happens, and $E2$ events should only be detected after any type of $E1$ event is triggered. This sequence can be accomplished by setting flags in the controller. Illustrated in Fig. 4 is the process of event detection. Afterwards, the $E1$ and $E2$ requests are handled by the SDN controller discussed in the next subsection.

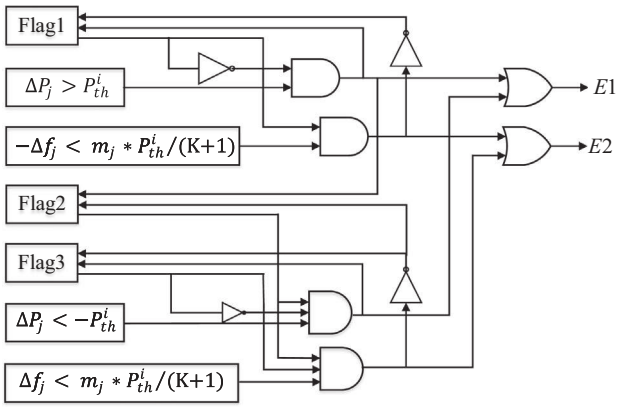

Fig. 4. The logic diagram of the event detection (all flags are initialized as zero).

3.2.2. SDN-based event-triggered communication

The SDN controller is a centralized communication network controller that has access to all the SDN switches. As shown in Fig. 5, three tables are stored and maintained in the SDN controller: the IP address table ($T1$), the microgrid cluster table ($T2$), and the communication state table ($T3$). These tables are updated when changes occur in the physical topology (e.g., one more microgrid joins the network) or in the communication configuration (e.g., add, delete or modify an IP address).

Using the IP protocol, each of the local controller's transceivers has a unique IP address which belongs to different microgrids and is stored in $T1$. Upon receiving a request, the SDN controller will check $T1$ to get the microgrid's index number. Assuming the number is i, then the SDN controller will check the ith element in $T2$, which is a table showing the K-NN information of each microgrid based on the electrical distance matrix. Each element in $T2$ is an index set defined as $\mathscr{K}_i$ for microgrid i, denoting all the K microgrids centered around it with close electrical distance. Table $T3$ is an $N \times N$ binary matrix initialized as zeros, which shows there is no global communication at the beginning. Since the communications are bidirectional, state table $T3$ is used to avoid repeated operations in the communication network. Specifically, for an $E1$ request from microgrid i, the SDN controller checks the ith row of $T3$ and find all zeros among the elements $\{i,k\},\ k \in \mathscr{K}_i$. If the elements on their diagonal positions are also zeros, it means there is no existing links between microgrid i and k. In this case, the SDN controller then generates instructions for the SDN switch to build the links and updates all zero elements on the ith row of $T3$ to ones. Similarly, for an $E2$ request, the SDN controller finds all nonzero elements on the ith row and checks if the elements on their diagonal position are zeros, indicating that the links are not requested by other events. Then the SDN controller can delete these links and update all one elements on the ith row to zeros. This process is illustrated in Fig. 6.

Compared with existing event-triggered approaches for ACA controllers, SDN-based event-triggered communication is realized directly in the network rather than on the local controllers. Specifically, the SDN switch can capture data packets from the leader DG units of the MG under power deficiency (or its recovery) and can forward them to its neighboring MGs. In contrast, the traditional way uses local controllers to broadcast data to their neighbors whenever events are detected. The benefits of using SDN here include the following: (1) it does not occupy controller-to-switch bandwidth, which always creates a bottleneck in the network; (2) it enables an adjustable neighboring microgrid set, which is maintained in $T2$ in the SDN controller; and (3) it is applicable to network configurations where single microgrids are in separate subnets.

4. Hardware-in-the-loop testing environment

This section will review the design and establishment of a cyber-physical HIL testbed to provide a realistic testing environment. We begin by introducing the high-level design of the cyber-physical HIL testbed, and we then specify the hardware components, NMGs models, and development of the SDN network.

4.1. The high-level design of the cyber-physical HIL testbed

In the HIL testbed, NMGs are simulated in real time on an OPAL-RT simulator; its cyber components (e.g., communication and event detection functions) are implemented on a group of virtual machines (VMs) running on three servers; and the data exchange is achieved through an SDN network.

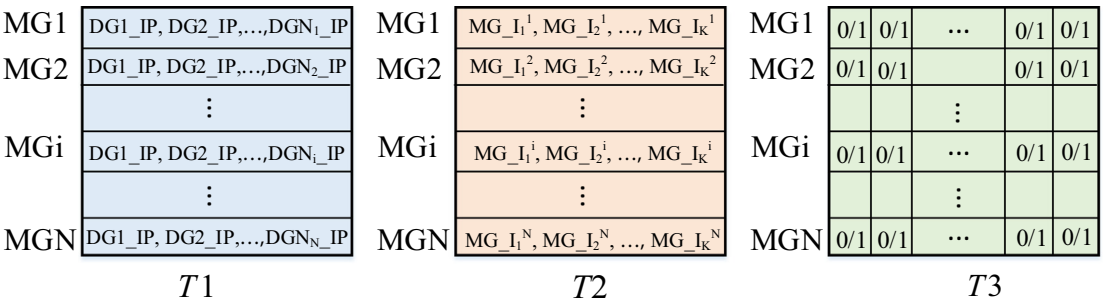

Fig. 5. The IP address table (*T*1), the microgrid cluster table (*T*2) and the communication state table (*T*3) in an SDN controller.

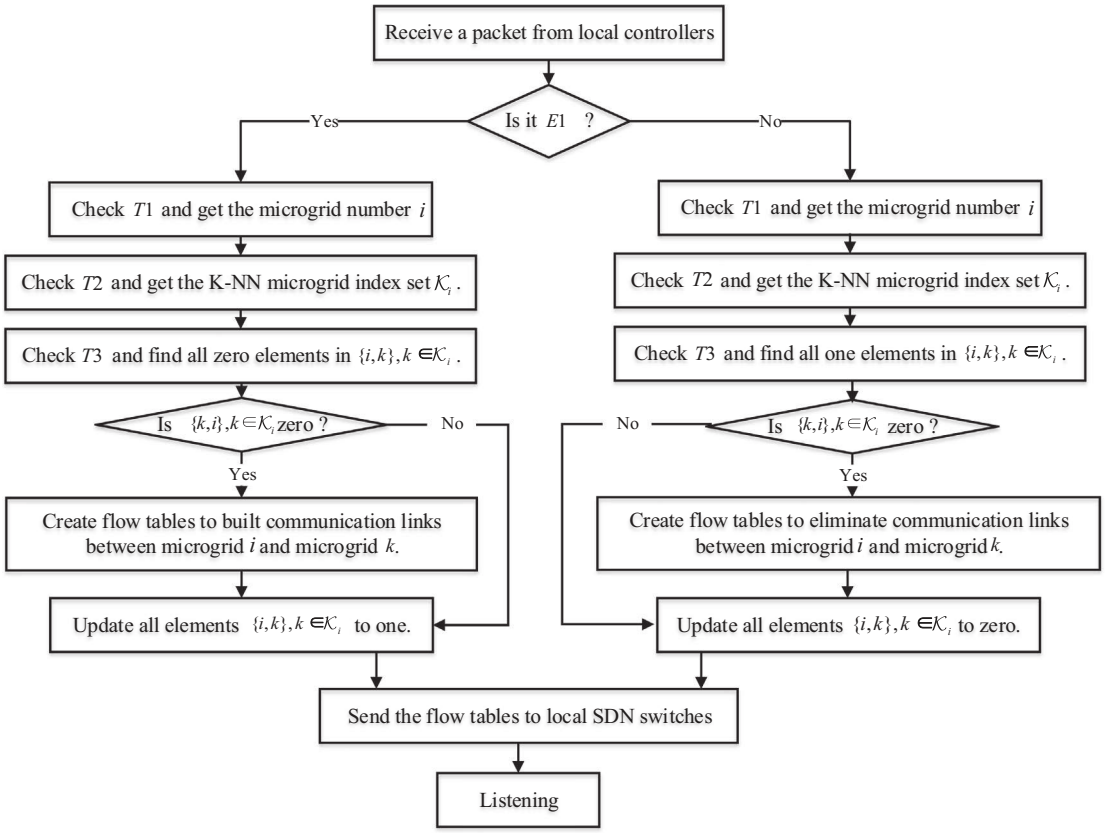

Fig. 6. Flow chart of SDN controller for event-triggered communication (the details of flow tables will be explained in Section 4).

The OPAL-RT simulator which is recognized for its high fidelity simulations of both the power grid and power electronics, has also been developed to incorporate communication performance either by communication simulators (co-simulation) [39] or by hardware (HIL) [24], using the asynchronous Ethernet blocks in RT-LAB (one software solver for OPAL-RT). Unlike co-simulation, in the HIL, data are transmitted through real communication platforms to study the impact of communication latency and contingencies on system response to various control functions. Therefore, in this paper, the hardware SDN switches are used to introduce the elements of a real-world communication environment and to support event-triggered data flow control, which is impossible to implement in a traditional non-SDN switch.

In order to emulate field data flows in the SDN network, the data traffic required in the power sharing control has to go through the hardware switches. Although the OPAL-RT simulator can have multiple Ethernet cards, data exchange among them is accomplished within the operation system resulting in a block of any external data exchange. For this reason, a group of VMs with independent IP and MAC addresses are added to receive data from the simulator, exchange data among each other, and send them back to the simulator. This approach only requires one or several host PCs

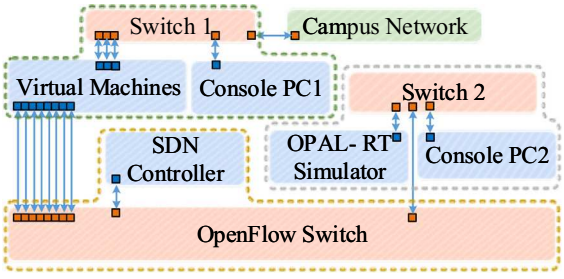

Fig. 7. The structure of the HIL testbed.

or servers, and it costs only CPU cycles and network card processing time, which is negligible compared with network latency.

As shown in Fig. 7, the above designed testbed consists of three functional groups: the real-time simulator and its auxiliary facilities (a console PC and a network switch); the eight VMs (hosted on three servers) and their auxiliary facilities (a console PC and a network switch); and the SDN network (an SDN controller and an OpenFlow switch). The three groups are connected through the SDN network and share a private Ethernet subnet. Meanwhile, each of the three servers has a management port, which is linked with the campus network through which their console PC is able to access all of the VMs. The cyber and physical components are illustrated in Fig. 8.

4.2. Real-time simulator and networked microgrids

In this paper, a 12-core simulator, OP5600, is used for a microseconds-level simulation running in real time. It provides a Gigabit Ethernet port for all IP-based communications including the connection with the console PC2 (via TCP/IP) and with the VMs (via UDP/IP). The console PC2 is used for model editing and compiling through the software solver, RT-LAB. To achieve real-time calculations, ARTEMiS-SSN [40] blocks are adopted to separate the state space of the networked microgrids model into 8 subspaces thus in order to calculate them on 8 cores in parallel.

The data exchange required by the power sharing control is achieved through multiple IP sockets, which are established on two dedicated cores to send and receive data from the VMs. In addition, they are automatically synchronized with the microgrids simulation through shared memory [24]. For each DG, its local measurement and control data (active power P_j, frequency f_j and secondary frequency control variable F_j) are fused into one packet and sent to the corresponding VM for event detection and data exchange.

The VMs are hosted on three servers (Dell PowerEdge R430), each of which has four Ethernet ports. One port is specifically used for the remote console PC1 and the rest are bounded with the 8 VMs on a one-to-one basis. Four instances of the same program are running on each VM to build four sockets linked with other VMs and the simulator. The event detection process (as shown in Fig. 4) is implemented on the VM. The $E1$ and $E2$ signals are sent to the SDN controller which then decides whether to establish or eliminate extra communication links.

The networked microgrids test case consists of four MGs, each of which has two Voltage Source Converter (VSC) interfaced DGs and two matched loads. The pulse-width modulation (PWM) signals of the VSCs are generated by the control blocks shown in Fig. 3. The DGs are connected to a local PCC bus, which is then integrated as a whole entity through the AC lines as shown in Fig. 9. The physical and control parameters are summarized in Table 1.

4.3. SDN-based event-triggered communication

In our HIL testbed, the SDN network consists of an SDN controller and an SDN switch running OpenFlow protocols. The Aruba 5406R switch is used for its ultra-low latency (less than 2.8 μs) and high processing speed (1.2 GHz). As shown in Fig. 7, among all ports on the OpenFlow switch, 8 ports are connected with 8 VMs, one port is linked with the simulator and one port is allocated to the SDN controller. In this paper, the SDN controller is developed using the Ryu framework as an application interface between the controller and the OpenFlow switch.

In the SDN controller, the IP address table ($T1$) is created. Based on the scale of the testbed, a two nearest neighbor microgrid cluster table ($T2$) is calculated using the parameters provided in Table 1. By checking the communication state table ($T3$), the SDN controller generates new flow rules in order to establish or eliminate data paths. This task is accomplished via a pipeline supported by the OpenFlow protocol.

The operation of the OpenFlow switch is carved by flow tables consisting of flow entries. The flow table matches the packets against the match fields (such as the source IP address) in its flow entries. Once a matched entry is found, the instructions (or flow rules) written in this entry will be executed. A pipeline is a set of flow tables operating in a forward-only order (shown in Fig. 10) predefined in their instruction sets. In this particular application of event-triggered communication, the SDN controller will define new instructions in the flow tables of the running pipeline and update the switch automatically to fulfill the control functions shown in Fig. 4.

For instance, once receiving the $E1$ request, the SDN controller creates new flow rules in the flow tables (1–K), such that they can forward specific data packets to the new IP addresses. Then

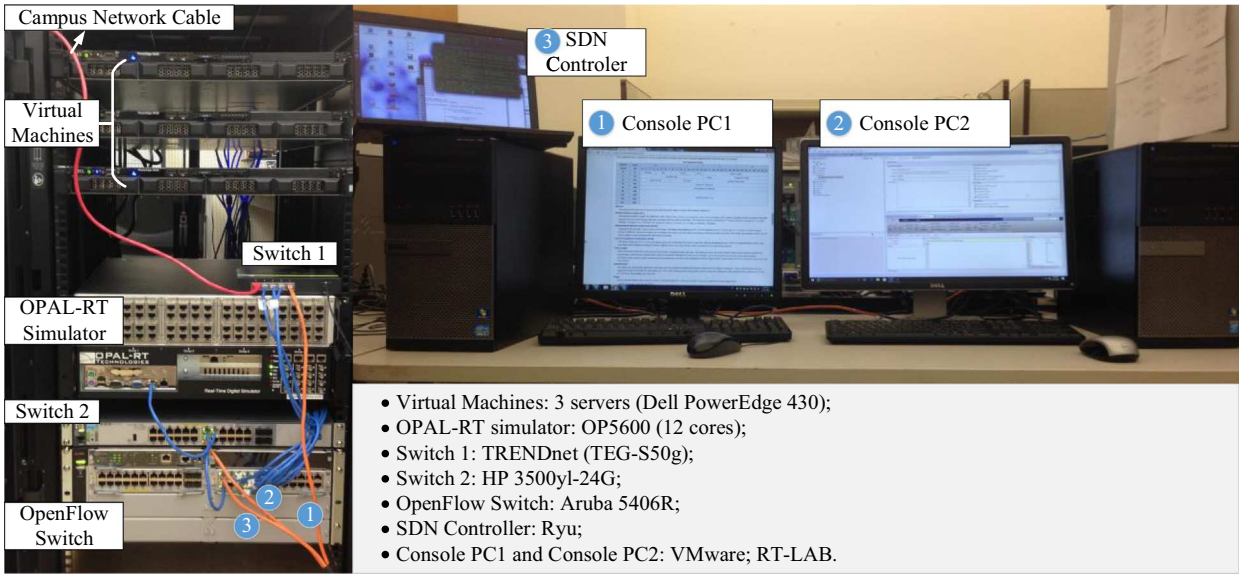

Fig. 8. The cyber and physical components of the HIL testbed.

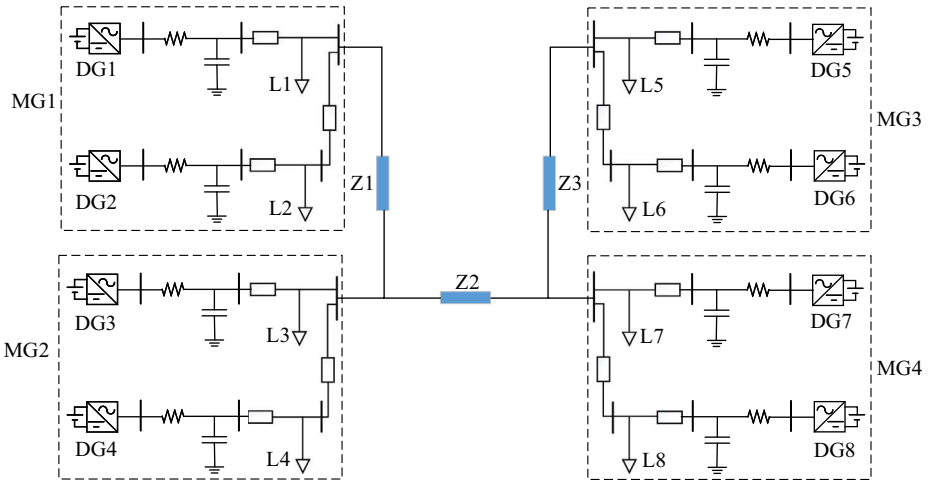

Fig. 9. The structure of the networked microgrids.

Table 1
Parameters for the networked microgrids.

Parameter	Value	
Nominal frequency	60 Hz	
DC voltage	800 V	
Nominal voltage	311 V (Line-Line RMS)	
Filter capacitance	50 μF	
Filter inductance	1.35 mH	
Line impedance Z1	R = 1 Ω, L = 10 mH	
Line impedance Z2	R = 5 Ω, L = 20 mH	
Line impedance Z3	R = 1 Ω, L = 10 mH	
–	Leader DGs (1, 3, 5, 7)	Follower DGs (2, 4, 6, 8)
Rated active power	10 kW	5 kW
Rated reactive power	5 kVar	2 kVar
Frequency droop Coeff.	0.6e−5 Hz/W	1.2e−5 Hz/W
Voltage droop Coeff.	1.2e−3 V/Var	2.4e−3 V/Var
Frequency restoration Coeff.	10	10
Local power sharing Coeff.	10	10
Global power sharing Coeff.	100	100

Note: (1) in this paper the uniform control parameters are used; (2) Coeff.: Coefficients.

the modified flow rules are sent out to the OpenFlow switch where they are activated immediately. Once this is done, when a packet arrives at the switch, it will go to the first table where it is forwarded to its original destination (Dest 0) indicated in its packet header. In the meantime, it is also passed to the next table where the destination IP in the packet header will be replaced with the IP address of the neighboring MG selected for global power sharing. A maximum of 2 × K new links (bidirectional communication) are established during this process. If this *E*1 request is from DG1 (MG1), the packets from DG1 to DG2 are forwarded to its two neighbors defined in *T*2, i.e. DG3 (MG2) and DG7 (MG4). Since the pipeline model and packet header modification are processed in the hardware OpenFlow switch, the event-triggered communication leads to negligible latency overhead (in microsecond level).

5. Experimental results

The NMGs' communication and distributed control strategy is tested on our cyber-physical HIL testbed. Different communication conditions are examined for single-event cases. The results show that the combination of global power sharing control, K-NN microgrid clustering, and SDN-based event-triggered communication has the best performance considering the communication cost and system response. Multiple-event cases then demonstrate the robustness of the SDN controller in dealing with a series of events, which are likely to occur in real NMG operations.

This section is organized into two studies on different power deficiency conditions designed to test system performance. The first study presented in Section 5.1, is *the single-event scenario* where one load (L1 in Fig. 9) in MG1 is increased from 10 kW to 15 kW initiating an *E*1 request from DG1. In the second study, Section 5.2 presents two different multiple-event scenarios*: the two separate events scenario* where both L1 and L3 are increased by 5 kW but at two time points that lead to no communication overlap, and *the two overlapped events scenario* where the same two

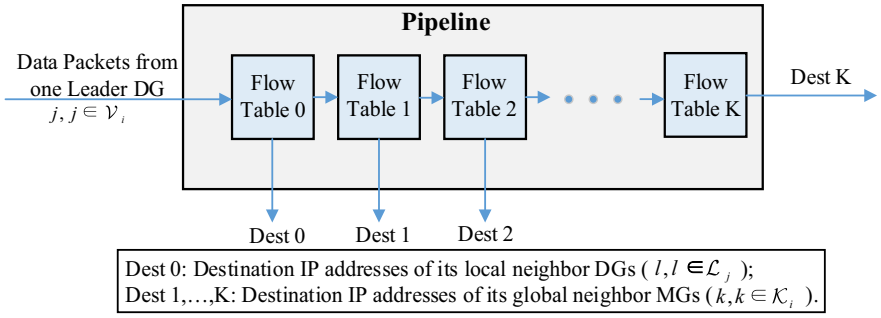

Fig. 10. Pipeline processing in the OpenFlow switch.

events happen at very similar time points which require synergized processing in the SDN controller. The results from the case studies are subsequently discussed to demonstrate the need for global power sharing, the effectiveness of K-NN microgrid clustering, the benefits of event-triggered communication, and the robustness of the controller in dealing with multiple-event scenarios.

The simulation settings for all cases include the following: a time step of 30 μs; a sample rate of 10 for communication data; uniform control parameters (shown in table 1); and a total simulation duration of 60 s. The DAPI-based secondary control starts at 1 s after the droop controllers reach their steady states. The discrete events are set up as follows: L1 increases at 6 s and recovers at 36 s; L3's increase occurs at 18 s and is restored at 48 s in the separate events case; and, in the overlapped events case, the increase of L3 is added at 6.6 s and removed at 36.6 s. Each microgrid has a power rating of 15 kW and thus the detection threshold P_{th} is set to 3 kW. Neighboring MG number K is selected as 2 based on the scale of the test case (only 4 MGs). The communication topologies used in different cases are illustrated in Fig. 11.

5.1. Study 1: Single-event scenario

5.1.1. Global power sharing controller validation

In order to illustrate the need for the global power sharing control, in Fig. 12(a) only the local power sharing control is enabled by the SDN network baseline configuration, and in Fig. 12(b) the global power sharing control is also enabled for comparison. As seen in Fig. 12(a), the two DGs in the same MG can exchange data to activate the local DAPI-based power sharing control. The results show that the power output of DG1 has an impulsive increase of 13.5 kW, and, with local power sharing, it converges to an approximate value of 12.5 kW. It is noticeable that the total supportive power generation of MG1 (DG1 and DG2) is 3.7 kW, which shows that the other MGs only contribute to a small amount of the total load increase (1.3 kW). In this case, the total demand for MG1 is above 120% of its power ratings, which indicates that MG1 is under an *emergency state* where it might lose the capability of supporting a further load change. This means that load shedding is needed to bring it back to a safe condition with enough local power reserve.

Meanwhile, in Fig. 12(b), bidirectional loop communication is applied to each of the four MGs' leader DGs, such that all of the MGs are participating in the global power sharing control, which leads to proportional power sharing (the same ratio with their power ratings) among all DGs. It can be observed that when the load is restored at 36 s, the output power of MG1 is increased by only 1.1 kW, approximately a quarter of the total load increase (1.25 kW). This implies that the global power sharing control is necessary to evenly distribute the demand increase among networked microgrids so that none of them runs into an emergency situation.

To further explain the two-layered power sharing control, the secondary frequency control variables for both cases are compared in Fig. 13. When there is only a local power sharing control (Eq. (2b)), the consensus algorithm will evenly distribute the power demand increase in L1 between DG1 and DG2. As shown in Fig. 13(a), only F_1 of DG1 and F_2 of DG2 can effectively respond to the demand change. On the contrary, with the proposed global power sharing (Eq. (4)), the leader DGs can boost their power generation within one second while the follower DGs can gradually follow up within 20 s as shown in Fig. 13(b). This is because the control signal F_j is first diffused among the leader DGs through a global consensus algorithm and then passed down to all of the follower DGs through the local consensus algorithm. This two-layered scheme can finally achieve a proportional allocation of the demand change among all DGs which requires only local controllers and global communication support.

Fig. 13(b) also indicates an important fact that MG2 (F_3, F_4) responds more quickly to an L1 change in MG1 than any of the other MGs. It reinforces the findings from Section 2.3.2 that strongly connected MGs converge more quickly. By using MG neighborhood sets, two-layered power sharing can be further improved as shown in the following study.

5.1.2. Effectiveness of K-NN-based microgrid clustering

In this study, the effectiveness of the K-NN based microgrid clustering approach is validated. The MG1's 2-NN MGs are selected by the electrical distance matrix, in order to reduce the number of participants in global power sharing from a loop communication of all MGs to a star communication centered at MG1. A comparison of Fig. 14(a) with Fig. 12(b) shows that communication among the 2-NN microgrid cluster (MG1, MG2, MG4) can achieve the same power sharing performance as that of an all-connected communication solution. It is noteworthy that even though MG3 is not included in communication, it still contributes to the final results due to its physical connection with other microgrids.

Furthermore, the results in Fig. 14(b) show that even 2-NN communication can be further reduced by limiting it to short time periods (shaded areas). The steady state power sharing of MG1 with event-triggered communication is almost the same but slightly lower than that of the continuous communication. This is because the secondary frequency control variable of DG1 finishes updating after the threshold Δf_j^{th} is satisfied (after 1 s), while, for continuous communication, it ends only when Δf_j reaches zero. This means that, with event-triggered communication, global power sharing can reach satisfactory results with a small deviation (depending on the value of Δf_j^{th}) from the results under continuous

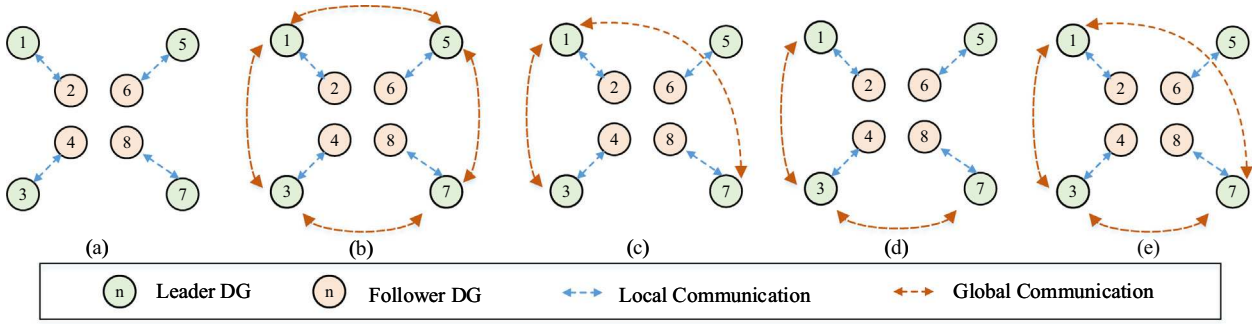

Fig. 11. SDN-based communication topologies: (a) Local communication within each microgrid (baseline communication for all cases); (b) Loop global communication involving all leader DGs; (c) Star global communication centered at DG1; (d) Star global communication centered at DG3; (e) Global communication requested simultaneously by DG1 and DG3.

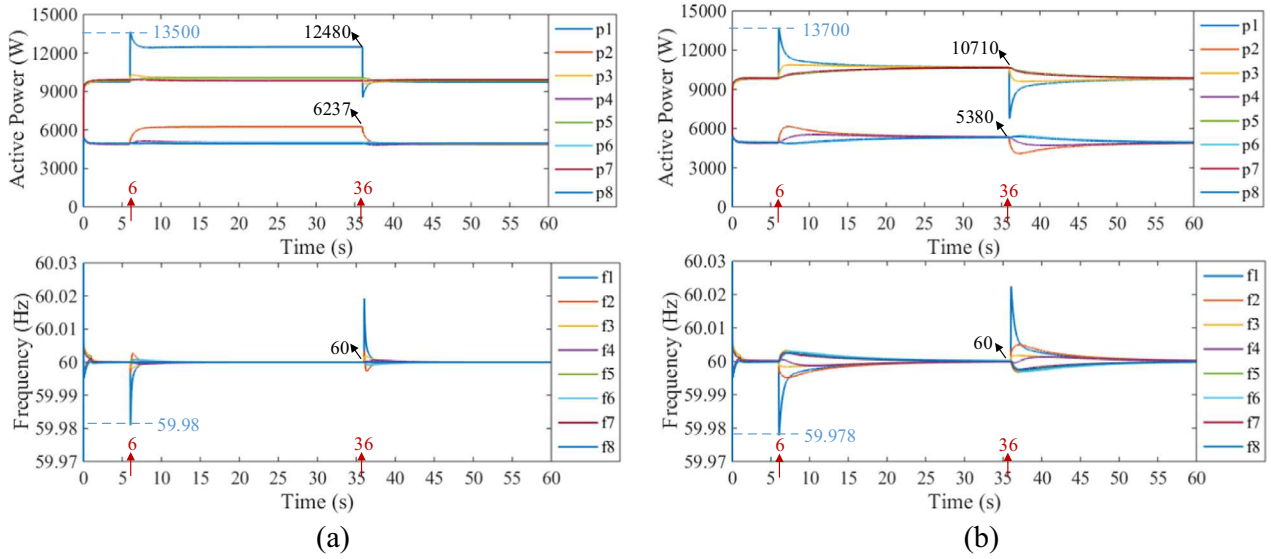

Fig. 12. (a) System response with only local power sharing control (Fig. 11(a)); (b) System response with global power sharing enabled by bidirectional loop communication among microgrids' leader DGs (Fig. 11(b)). (Note: the power outputs of DG1 and DG2 and the system frequency before load recovery are labeled on both in this figure and Fig. 14 to show the steady state power sharing results.)

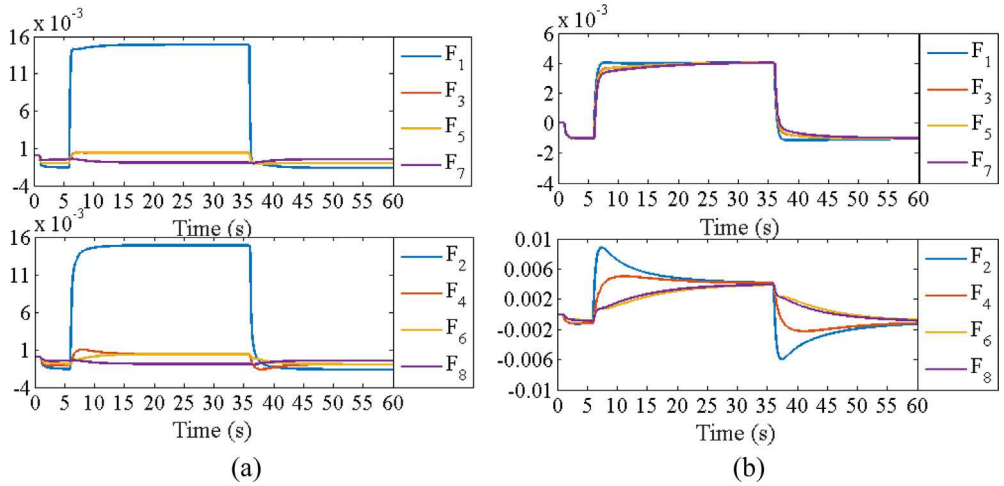

Fig. 13. Secondary frequency control variables F_j for all DGs: (a) In the case of Fig. 12(a); (b) In the case of Fig. 12(b) (the upper subplots for leader DGs and the lower for follower DGs).

communication. This deviation can be totally eliminated by enabling the exchange of sparse data packets after an *E*2 request instead of canceling the global communication. Since our target is to solve the local power deficiency with minimum cost, the presented communication shows the best trade-off performance. This can be elaborated in greater detail by comparing control signals in both cases.

The control signals for power sharing with continuous communication and for event-triggered communication are compared in Fig. 15. The shaded areas mark the integration of the signals, which are their (negative) contributions to the final secondary frequency control variable (F_1). It is shown that both the frequency restoration and local consensus control signals attempt to boost F_1 following a load increase, while the global consensus signal tries to slow down this process by averaging F_1 with $F_i,\ i \in \mathcal{K}_i$ (the leader DGs in neighboring MGs).

The comparison of Fig. 15(a) and (b) shows that, despite an instantaneous impulse caused by event-triggered communication, this spike does not have accumulative effect and thus does not affect the stabilized secondary frequency control variable. After the communication is eliminated, the local controller will keep using the last F_i received, and this prevents the neighboring MGs from further power adjustment after the power deficiency or recovery issue is resolved. This is a favorable outcome for real-world applications.

In conclusion, this subsection shows that the proposed two-layered power sharing control can be implemented on K-NN microgrid clusters using event-triggered communication without diminishing its power sharing performance. In this way, the control and communication costs for achieving fast power support among NMGs are drastically reduced.

5.1.3. Performance of SDN-based event-triggered communication

Studies in this subsection illustrate the performance of SDN-based event-triggered communication. Four communication sockets are created in each VM: Socket1 collects data from the simulator and passes them to its local neighboring VM (DG); Socket2 receives data from the local neighbor and forwards them back to

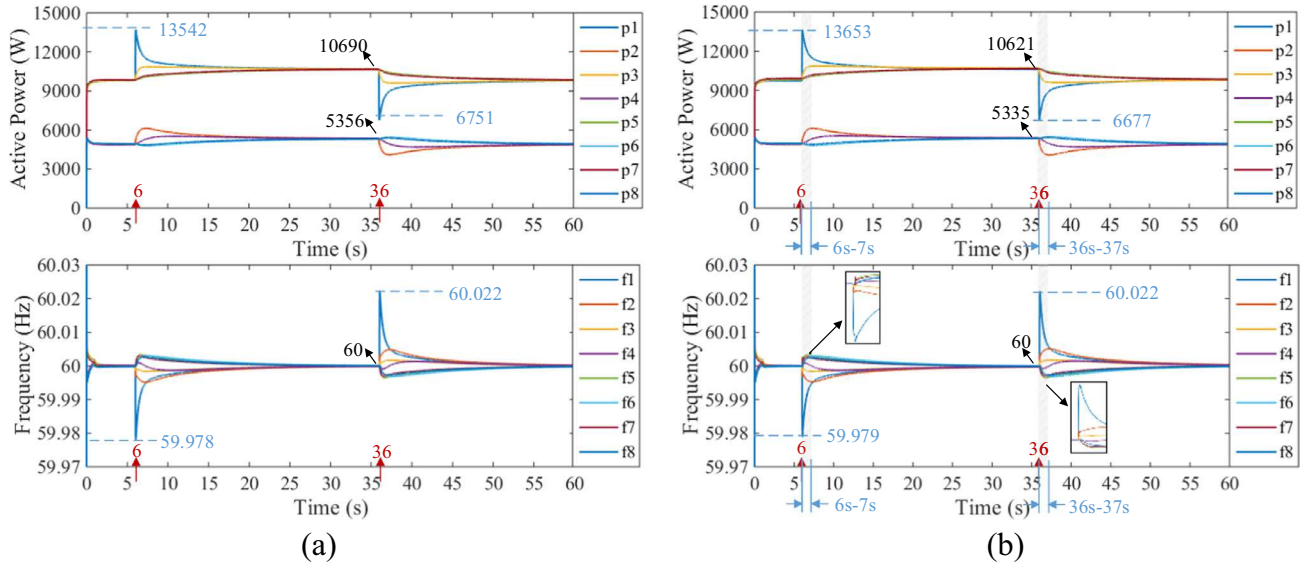

Fig. 14. System response with global power sharing among two nearest neighbors (2-NN) of MG1(Fig. 11(c)) enabled by: (a) Continuous communication; (b) Event-triggered communication.

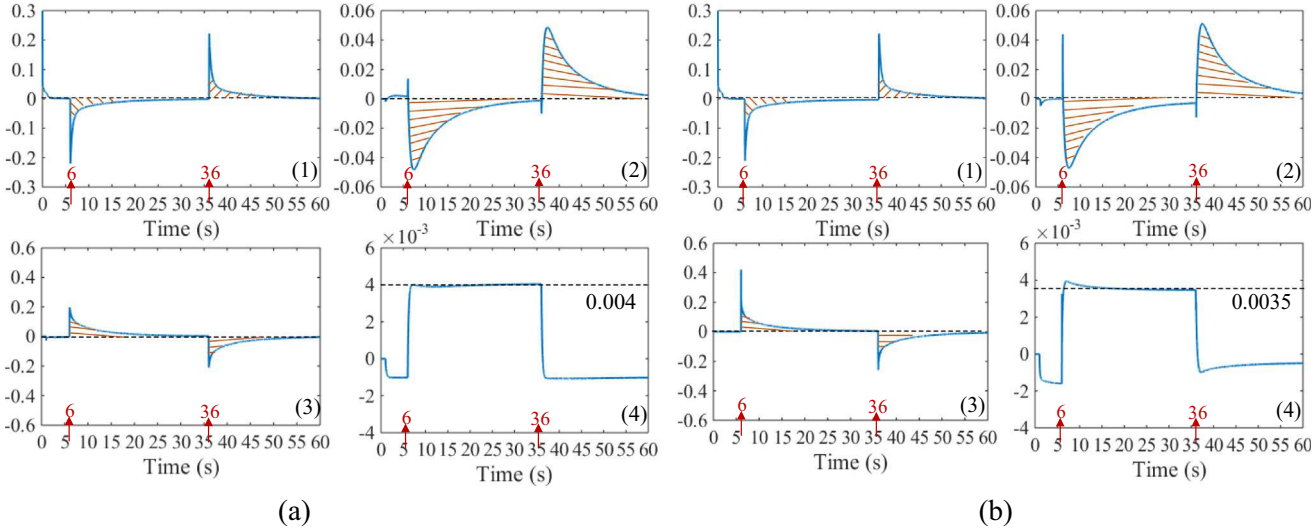

Fig. 15. Control signals of DG1: (a) in the case of Fig. 14(a); (b) in the case of Fig. 14(b). Note: (1) Frequency Restoration Control Signal; (2) Local Consensus Control Signal; (3) Global Consensus Control Signal; (4) Secondary Frequency Control Variable.

the simulator; Socket3 and Socket4 await data from the pipeline flow tables, which are executed in the OpenFlow Switch and updated dynamically by the SDN controller. As an example, the data flows of VM1 are depicted in Fig. 16(a) where the solid lines are the data related to local power sharing (Fig. 11(a)) and the dashed lines are the potential data flows required by global power sharing control (Fig. 11(b–e)).

To illustrate the changes in local traffic during the event-triggering process in Fig. 14(b), the data throughput of VM1 are recorded and shown in Fig. 16(b). At 6 s, the detection function running on Socket1 of VM1 identifies a power deficiency condition and sends the $E1$ request to the SDN controller. The SDN controller checks tables to obtain its two neighbors (MG2 and MG4) and subsequently creates two flow rules in the pipeline to add two data flows: DG1 ↔ DG3 and DG1 ↔ DG7 (Fig. 11(c)). Immediately after receiving the flow rules, the OpenFlow Switch creates new traffic to enable information sharing among the selected microgrids. These new links are canceled when the SDN controller receives the $E2$ signal indicating that power is already properly shared. The Wireshark (a network monitoring tool) is adopted to collect all packets in VM1 every 100 ms. Test results show that its throughput is doubled from 6 s to 7 s and from 36 s to 37 s, demonstrating the two extra links added on the local traffic during the global sharing process. Compared with the continuous data exchange, the event-triggered communication only requires a short period (one second for each event) of global traffic, which requires minimum bandwidth usage.

5.2. Study 2: Multiple-events scenario

In this study, two cases are tested to show the response of the SDN controller to multiple-events with or without overlap in their request periods. In Fig. 17(a), the shaded areas show the four time slots with global communication. DG1 and DG3 send requests at 6 s and 18 s respectively and their global power sharing ends within 1second. Although it is less likely that two power deficiency

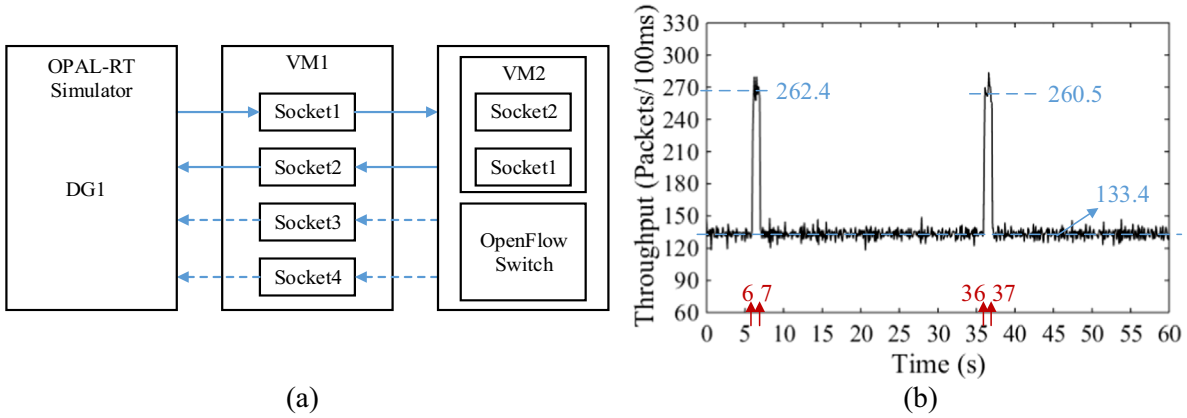

Fig. 16. (a) All data flows of VM1 (representing DG1); (b) Data throughput of VM1 during event-triggered communication.

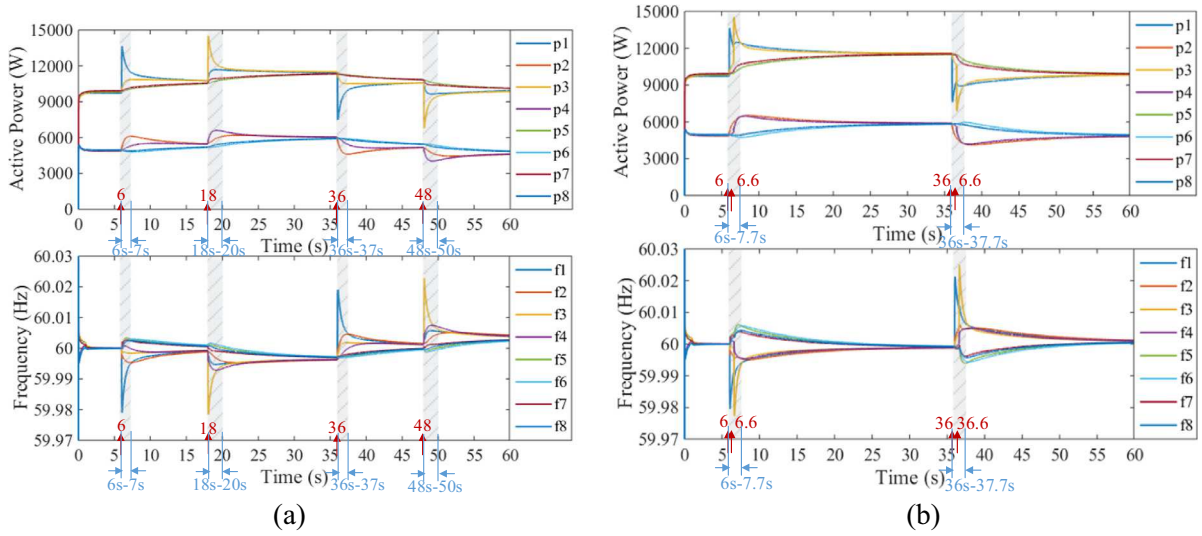

Fig. 17. (a) Two separate events that have no communication overlap (Fig. 11(c) and (d)); (b) Two overlapped events that have a shared communication link (Fig. 11(e)).

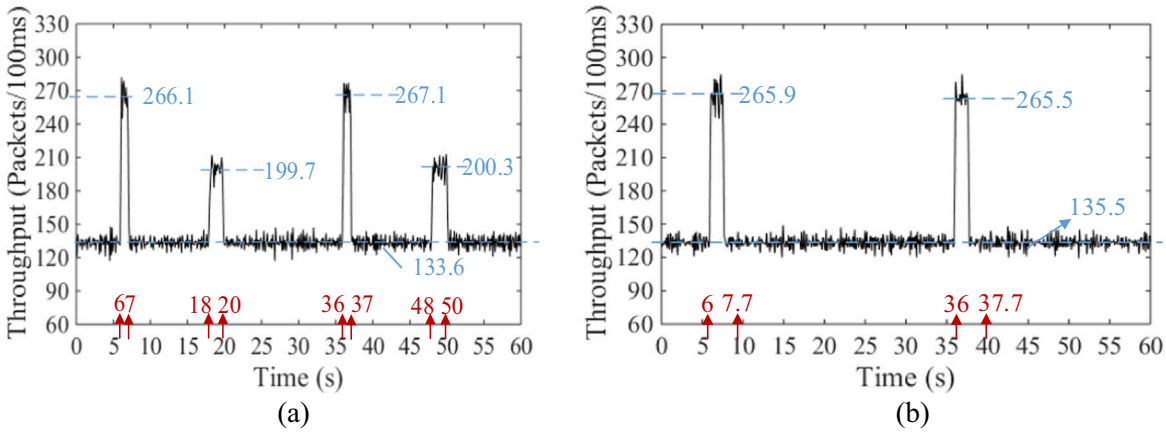

Fig. 18. (a) Data throughput of VM1 during two separate events; (b) Data throughput of VM1 during two overlapped events.

contingencies will occur within one second, it is necessary to study the SDN controller's capability of dealing with such instances. In Fig. 17(b), the L3 load increase happens just 0.6 s after the L1 increase occurs, which triggers global communication in MG2 and extends the global power sharing of MG1 to 9.3 s. By the end of the power sharing process, each microgrid contributes approximately 2.5 kW to the total load increase of 10 kW.

The data flows involved in the multiple-events scenario is analyzed to gain insight into the event-triggered process. The communications requested by MG1 are DG1 ↔ DG3 and DG1 ↔ DG7

(Fig. 11(c)) while those requested by MG2 are DG1 ↔ DG3 and DG3 ↔ DG7 (Fig. 11(d)). Thus, DG1 will establish two global links during the first event but only one global link for the second. As a result, for the two separate events scenario, as shown in Fig. 18 (a), the data throughput of VM1 (DG1) is doubled during 6 s to 7 s and 36 s to 37 s when MG1 sends its request, but is increased by 50% during 18 s to 20 s and 48 s to 50 s when MG2 sends its request.

The sequence of event requests for the overlapped events is: ① *E*1 from VM1, ② *E*1 from VM3, ③ *E*2 from VM1, ④ *E*2 from VM3, ⑤ *E*1 from VM1, ⑥ *E*1 from VM3, ⑦ *E*2 from VM3, and ⑧ *E*2 from VM1. Since the occurrences of these two events are very close (an interval of 0.6 s), the data throughput shows no change during period from 6 s (①) to 7.7 s (④) and from 36 s (⑤) to 37.7 s (⑧), where it keeps twice of the baseline value (see Figs. 18(b) and 11(e)).

The results in this study indicate that the SDN controller is able to avoid repetitive operations in the network and conflict among multiple requests. This validates the event detection and processing design presented in Section 3.2.

To implement the proposed methods in real-world microgrid applications, three steps are to be performed for the hardware infrastructure: (1) add a global power sharing control and communication interface in selected leader DGs (Fig. 3); (2) add event detection blocks in local DGs (Fig. 4); and (3) upgrade the existing communication network to an SDN network. The first two are easy to accomplish, especially when the DGs are already equipped with local power sharing controllers. The last step is also well developed in the area of SDN either through software (low cost) upgrades or hardware replacements. These three steps enable microgrid plug-and-play in the NMGs system under our control and communication architecture. Thus, the SDN-enabled methods are cost-effective and scalable, offering promising microgrid solutions for future smart cities and smart and connected communities.

6. Conclusion

This paper pioneers the use of SDN in NMGs by leveraging the programmability and flexibility of the SDN architecture to enable highly resilient NMGs. A layered power-sharing scheme is developed for NMGs, supported by SDN-based event-triggered communication. The method is fully distributed and only requires an additional global power-sharing block on the local controller of the leader DGs. To further minimize the communication cost, a K-NN microgrids set is selected using electrical distance information, and an event-triggered communication scheme is established using an SDN network. As a result, only during the power deficiency and power recovery events is the global communication enabled, which significantly reduces bandwidth usage. It also mitigates the risks of catastrophic congestion on both backbone communication networks and controller-to-switch data paths. Therefore, resilient NMGs operations such as distributed power sharing are assured. Case studies on a novel HIL NMG testbed have illustrated that global power sharing among four NMGs can be achieved through local controllers with only one to two seconds of global communication at each event.

Although the SDN-based cyber architecture in this paper is designed for networking microgrids, the same methodology can be used to establish more resilient networked control systems. Future work is required to further understand the capabilities and limits of the SDN architecture in integrating complex energy systems containing energy storage devices and distributed energy resources, underpinned by theoretical analyses and experimental studies.

Acknowledgement

This material is based upon work supported by the National Science Foundation under Grant Nos. 1647209 and 1611095.

We would like to thank Emma Burris-Janssen for proofreading the manuscript.

References

[1] Sreedharan P, Farbes J, Cutter E, Woo CK, Wang J. Microgrid and renewable generation integration: University of California. San Diego. Appl Energy 2016;169:709–20. http://dx.doi.org/10.1016/j.apenergy.2016.02.053.

[2] Marnay C, Venkataramanan G, Stadler M, Siddiqui AS, Firestone R, Chandran B. Optimal technology selection and operation of commercial-building microgrids. IEEE Trans Power Syst 2008;23:975–82. http://dx.doi.org/10.1109/TPWRS.2008.922654.

[3] Ma X, Wang Y, Qin J. Generic model of a community-based microgrid integrating wind turbines, photovoltaics and CHP generations. Appl Energy 2013;112:1475–82. http://dx.doi.org/10.1016/j.apenergy.2012.12.035.

[4] Li M, Zhang X, Li G, Jiang C. A feasibility study of microgrids for reducing energy use and GHG emissions in an industrial application. Appl Energy 2016;176:138–48. http://dx.doi.org/10.1016/j.apenergy.2016.05.070.

[5] Guerrero JM, Vasquez JC, Matas J, De Vicuña LG, Castilla M. Hierarchical control of droop-controlled AC and DC microgrids – a general approach toward standardization. IEEE Trans Ind Electron 2011;58:158–72. http://dx.doi.org/10.1109/TIE.2010.2066534.

[6] Haddadian H, Noroozian R. Multi-microgrids approach for design and operation of future distribution networks based on novel technical indices. Appl Energy 2017;185:650–63. http://dx.doi.org/10.1016/j.apenergy.2016.10.120.

[7] Bie Z, Zhang P, Li G, Hua B, Meehan M, Wang X. Reliability evaluation of active distribution systems including microgrids. IEEE Trans Power Syst 2012;27:2342–50. http://dx.doi.org/10.1109/TPWRS.2012.2202695.

[8] Cheung K. DOE perspective on microgrids. IEEE appl power electron conf expo; 2015. http://www.apec-conf.org/Portals/0/Plenary%20Presentations/Speaker%204%20Kerry%20Cheung%20PRES.pdf [accessed 2017.05.11].

[9] Shahnia F, Chandrasena RPS, Rajakaruna S, Ghosh A. Autonomous operation of multiple interconnected microgrids with self-healing capability. IEEE Power Energy Soc. Gen. Meet. 2013. http://dx.doi.org/10.1109/PESMG.2013.6672794.

[10] Lasseter RH. Smart distribution: coupled microgrids. Proc IEEE 2011;99:1074–82. http://dx.doi.org/10.1109/JPROC.2011.2114630.

[11] Hossain MJ, Mahmud MA, Milano F, Bacha S, Hably A. Design of robust distributed control for interconnected microgrids. IEEE Trans Smart Grid 2016;7:2724–35. http://dx.doi.org/10.1109/TSG.2015.2502618.

[12] Fang X, Yang Q, Wang J, Yan W. Coordinated dispatch in multiple cooperative autonomous islanded microgrids. Appl Energy 2016;162:40–8. http://dx.doi.org/10.1016/j.apenergy.2015.10.076.

[13] Li J, Ma XY, Liu CC, Schneider KP. Distribution system restoration with microgrids using spanning tree search. IEEE Trans Power Syst 2014;29:3021–9. http://dx.doi.org/10.1109/TPWRS.2014.2312424.

[14] Wang Z, Chen B, Wang J, Chen C. Networked microgrids for self-healing power systems. IEEE Trans Smart Grid 2016;7:310–9. http://dx.doi.org/10.1109/TSG.2015.2427513.

[15] Yuen C, Oudalov A, Timbus A. The provision of frequency control reserves from multiple microgrids. IEEE Trans Ind Electron 2011;58:173–83. http://dx.doi.org/10.1109/TIE.2010.2041139.

[16] Lv T, Ai Q. Interactive energy management of networked microgrids-based active distribution system considering large-scale integration of renewable energy resources. Appl Energy 2016;163:408–22. http://dx.doi.org/10.1016/j.apenergy.2015.10.179.

[17] Kou P, Liang D, Gao L. Distributed EMPC of multiple microgrids for coordinated stochastic energy management. Appl Energy 2017;185:939–52. http://dx.doi.org/10.1016/j.apenergy.2016.09.092.

[18] He J, Li Y, Liang B, Wang C. Inverse power factor droop control for decentralized power sharing in series-connected micro-converters based islanding microgrids. IEEE Trans Ind Electron 2017. http://dx.doi.org/10.1109/TIE.2017.2674588.

[19] Wang C, Li Y, Peng K, Hong B, Wu Z, Sun C. Coordinated optimal design of inverter controllers in a micro-grid with multiple distributed generation units. IEEE Trans Power Syst 2013;28:2679–87. http://dx.doi.org/10.1109/TPWRS.2013.2245922.

[20] Coelho VN, Cohen MW, Coelho IM, Liu N, Guimarães FG. Multi-agent systems applied for energy systems integration: State-of-the-art applications and trends in microgrids. Appl Energy 2017;187:820–32. http://dx.doi.org/10.1016/j.apenergy.2016.10.056.

[21] Dörfler F, Simpson-Porco JW, Bullo F. Breaking the hierarchy: distributed control and economic optimality in microgrids. IEEE Trans Control Netw Syst 2016;3:241–53. http://dx.doi.org/10.1109/TCNS.2015.2459391.

[22] Simpson-Porco JW, Shafiee Q, Dorfler F, Vasquez JC, Guerrero JM, Bullo F. Secondary frequency and voltage control of islanded microgrids via distributed averaging. IEEE Trans Ind Electron 2015;62:7025–38. http://dx.doi.org/10.1109/TIE.2015.2436879.

[23] Guo F, Wen C, Mao J, Song YD. Distributed secondary voltage and frequency restoration control of droop-controlled inverter-based microgrids. IEEE Trans Ind Electron 2015;62:4355–64. http://dx.doi.org/10.1109/TIE.2014.2379211.
[24] Ren L, Qin Y, Wang B, Zhang P, Luh PB, Jin R. Enabling resilient microgrid through programmable network. IEEE Trans Smart Grid 2016. http://dx.doi.org/10.1109/TSG.2016.2589903.
[25] Koldehofe B, Dürr F, Tariq MA. Tutorial: event-based systems meet software-defined networking. In: Proc 7th ACM int conf distrib event-based syst – DEBS '13, 2013. p. 271. 10.1145/2488222.2488270.
[26] Yuan Y, Lin D, Alur R, Loo BT. Scenario-based programming for SDN policies. In: Conex '15 Proc 11th ACM conf emerg netw exp technol; 2015. 10.1145/2716281.2836119.
[27] McClurg J, Hojjat H, Foster N, Černý P. Event-driven network programming. ACM SIGPLAN Not 2016;51:369–85. http://dx.doi.org/10.1145/2980983.2908097.
[28] Wang X, Lemmon MD. Event-triggering in distributed networked control systems. IEEE Trans Automat Contr 2011;56:586–601. http://dx.doi.org/10.1109/TAC.2010.2057951.
[29] Seyboth GS, Dimarogonas DV, Johansson KH. Event-based broadcasting for multi-agent average consensus. Automatica 2013;49:245–52. http://dx.doi.org/10.1016/j.automatica.2012.08.042.
[30] Kia SS, Cortés J, Martínez S. Distributed event-triggered communication for dynamic average consensus in networked systems. Automatica 2015;59:112–9. http://dx.doi.org/10.1016/j.automatica.2015.06.011.
[31] Ainsworth N, Grijalva S. A structure-preserving model and sufficient condition for frequency synchronization of lossless droop inverter-based AC networks. IEEE Trans Power Syst 2013;28:4310–9. http://dx.doi.org/10.1109/TPWRS.2013.2257887.
[32] Simpson-Porco JW, Dörfler F, Bullo F. Synchronization and power sharing for droop-controlled inverters in islanded microgrids. Automatica 2013;49:2603–11. http://dx.doi.org/10.1016/j.automatica.2013.05.018.
[33] He J, Li YW. An enhanced microgrid load demand sharing strategy. IEEE Trans Power Electron 2012;27:3984–95. http://dx.doi.org/10.1109/TPEL.2012.2190099.
[34] Mahmood H, Michaelson D, Jiang J. Accurate reactive power sharing in an islanded microgrid using adaptive virtual impedances. IEEE Trans Power Electron 2015;30:1605–17. http://dx.doi.org/10.1109/TPEL.2014.2314721.
[35] Ahumada C, Cárdenas R, Sáez D, Guerrero JM. Secondary control strategies for frequency restoration in islanded microgrids with consideration of communication delays. IEEE Trans Smart Grid 2016;7:1430–41. http://dx.doi.org/10.1109/TSG.2015.2461190.
[36] Coelho EAA, Wu D, Guerrero JM, Vasquez JC, Dragičević T, Stefanović Č, et al. Small-signal analysis of the microgrid secondary control considering a communication time delay. IEEE Trans Ind Electron 2016;63:6257–69. http://dx.doi.org/10.1109/TIE.2016.2581155.
[37] Bliman PA, Ferrari-Trecate G. Average consensus problems in networks of agents with delayed communications. Automatica 2008;44:1985–95. http://dx.doi.org/10.1016/j.automatica.2007.12.010.
[38] Cotilla-Sanchez E, Hines PDH, Barrows C, Blumsack S, Patel M. Multi-attribute partitioning of power networks based on electrical distance. IEEE Trans Power Syst 2013;28:4979–87. http://dx.doi.org/10.1109/TPWRS.2013.2263886.
[39] Bian D, Kuzlu M, Pipattanasomporn M, Rahman S, Wu Y. Real-time co-simulation platform using OPAL-RT and OPNET for analyzing smart grid performance. IEEE Power Energy Soc. Gen. Meet. 2015. http://dx.doi.org/10.1109/PESGM.2015.7286238.
[40] The state-space nodal solver for ARTEMiS; 2016. http://www.opal-rt.com/solver-artemis-ssn/ [accessed 2017.03.31].